

Finite key effects in satellite quantum key distribution

Jasminder S. Sidhu,* Thomas Brougham,* Duncan McArthur, Roberto G. Pousa, and Daniel K. L. Oi[†]

SUPA Department of Physics, University of Strathclyde, Glasgow, G4 0NG, United Kingdom

(Dated: 26th June 2022)

Quantum key distribution (QKD) can provide secure means of communication that are robust to general quantum computing attacks. Satellite QKD (SatQKD) presents the means to overcome range limitations in fibre optic-based systems and achieve global coverage but raises a different set of challenges. For low-Earth orbit SatQKD, a major limitation is the restricted time window for quantum signal transmission and highly variable channel loss during a satellite overpass of an optical ground station. Here, we provide a systematic analysis of the finite block size effects on secret key length generation for low latency operation using BB84 weak coherent pulse decoy state protocols. In particular, we look at how the achievable single pass secret key length depends on various system parameters for different overpass geometries and calculate the total long-term-average key length. We find that optimisation of basis bias, pulse probabilities and intensities, and data selection, is crucial for extending the range of satellite trajectories and link efficiencies for which finite-block size keys can be extracted. The results also serve as a guide for system sizing of future SatQKD systems and the performance levels required for sources and detectors.

I. INTRODUCTION

The second quantum revolution promises to deliver new technologies operating at the fundamental limits of Physics that offer enhanced capabilities over conventional classical devices [1]. These include quantum sensors [2–4], secure quantum communications [5, 6], and quantum computers that open up new computational paradigms and facilitate a speed-up of particular problems [7, 8]. A quantum communication infrastructure could network quantum devices, creating the quantum internet [9] while also enabling distributed quantum sensors [10–13], clocks [14, 15], and navigation systems [16]. However, creating the necessary long distance links is a considerable challenge, since exponential absorption in optical fibres places severe limits for direct transmission of quantum photonic signals to under 1000 km with the most recent records still falling significantly short of that limit [17–20].

Quantum repeaters have been proposed as a method of overcoming the direct transmission limit but are still in the early stages of development with long-distance deployment likely to be over a decade away [21]. Hence, alternative methods of spanning intercontinental and global distances are required. Satellite-based quantum communication systems [22–27] is such a method that has received considerable recent interest with the pioneering proof-of-concept in-orbit demonstrations by Micius particularly noteworthy [28].

Space-ground quantum communication introduces particular challenges. Low-Earth orbit satellites have a limited time window in which they can contact an optical ground station in order to establish and maintain a quantum channel. For satellite quantum key distribution (SatQKD), this is particularly acute as protocols typically assume large amounts of data transfer from which a secret key is extracted. This asymptotic resource assumption, where statistical uncertainties of the channel parameters are assumed negligible, is impractical. In contrast, if the quantum transmission data is limited,

then the security of the final secret key rests on a thorough treatment of statistical fluctuations in the estimation of key quantities, such as the phase error rate and number of received single photon signals [29–31].

With limited data, there is also a trade-off between the amount of received signal sacrificed for parameter estimation and the remaining raw key for further processing. This exacerbates the problem of secret key distillation. Further post-processing operations, such as error correction, reduce the amount of extractable secret key, with small block lengths leading to additional inefficiencies over the asymptotic limit [32, 33].

To date, there has been little systematic analysis of achievable secret key lengths that take into account finite block size effects in SatQKD. Initial SatQKD studies employed the standard deviation of measured quantities to estimate statistical uncertainty [34, 35]. These were used to derive upper and lower bounds on the gain and phase error rate of the received single photons in order to derive correction terms to the secret key rate. More rigorous methods were developed to account for statistical fluctuations based in smooth entropies [29] leading to better finite-key bounds [36] and their application to free-space quantum communication [37]. Recently, tight bounds [33] and small block length analyses [38] for QKD have been developed, which further improves the achievable rates with restricted amounts of signal.

Here, we apply recent results to estimate the achievable secret key length from minimal number of satellite overpasses, ideally a single pass. Our study accounts for different satellite trajectories, realistic descriptions for the sources and detectors, and quantum link efficiencies comparable with experimental demonstrations from the Micius satellite. We include practical finite key statistics to determine the optimised key rates per pass for WCP-source QKD protocols, comparing the performance of symmetric and asymmetric variants. We also investigate the influence of different system characteristics on the secret key length.

For simplicity, the majority of the presented results are for a zenith overpass, though our analysis can consider any pass geometry and optimising protocol parameters such as biases and

* These two authors contributed equally

[†] daniel.oi@strath.ac.uk

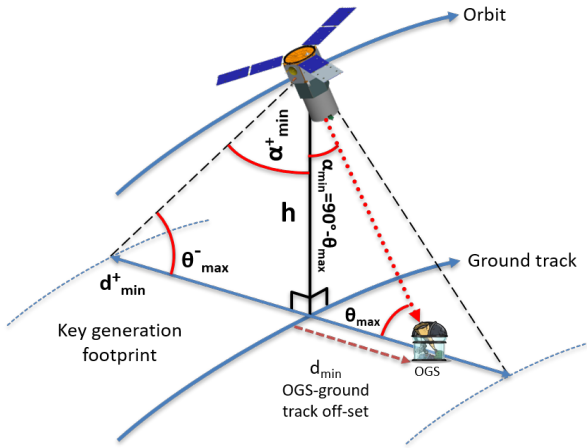


Figure 1. Geometry of satellite pass. We consider a satellite in a circular sun synchronous orbit at an altitude h . The ground track of the satellite passes the OGS with a minimum distance of d_{\min} and reaches a maximum elevation of θ_{\max} , the corresponding minimum zenith angle is $\alpha_{\min} = 90^\circ - \theta_{\max}$. We define the smallest θ_{\max} for which a key can be generated as θ_{\max}^+ , this defines the footprint width of the satellite within which an OGS passing through can establish a finite key. A comprehensive model of satellite-OGS orbital geometry can be found in [39].

intensities to maximise the secret length that can be generated. We compare the annual average secret key length for different system link efficiencies and quantify the improvement of normalised (per pass) secret key we can generate from combining data from multiple satellite passes, extending the range of acceptable system link efficiencies and increasing the key length per pass. Our work serves as the basis for preliminary SatQKD system sizing and performance analysis and when combined with a size vs cost models, helps determine the optimum OGS size for a fixed space segment.

II. SYSTEM MODEL

We consider a satellite in a circular low Earth Sun-synchronous orbit of altitude $h = 500$ km, similar to the Micius satellite [28]. We perform downlink QKD operations during night overpasses of the optical ground station to reduce errors due to background light. Our simulation generates time, elevation, and range, as a function of different angles between the orbital plane and that of the optical ground station (OGS) that represents different ground track off-sets and maximum elevations for the overpass (Fig. 1). We simulate the time from when the satellite is first visible above 0° elevation until it passes below 0° and calculate the instantaneous link efficiency depending on the elevation and range in order to generate expected detector count statistics.

We simplify our model by combining all losses into a single link efficiency value $\eta_{\text{link}} = -10 \log_{10} p_d$ (dB). This characterises the probability p_d that a single photon transmitted by the satellite is detected. A lower dB value of η_{link} represents better

Description	Parameter	Value
Intrinsic QBER	QBER_I	5×10^{-3}
Afterpulse probability	p_{ap}	1×10^{-3}
Extraneous count probability/pulse	p_{ec}	5×10^{-7}
Source Rate	N	1×10^8 Hz
Correctness parameter	ϵ_c	10^{-15}
Secrecy parameter	ϵ_s	10^{-9}
System link efficiency	$\eta_{\text{link}}^{\text{sys}}$	27 dB
Altitude	h	500 km

Table I. Parameters and their values that are used in the numerical optimisation of the finite key rate. A description for the channel link efficiency, η_{link} , is given in the main text. The error correction efficiency is estimated as a function of block size [32]. The QBER_I value of 0.5% is consistent with the reported results from Micius [17]. The extraneous count rate is the sum of the detector dark count and background rate. A reported background count rate 500 – 2000 cps per detector, depending on the position of the moon [40], leads to a probability per pulse of 5×10^{-7} taking the best case value with detector dark count being a less significant contribution. (an order of magnitude lower). With a source rate of 100 MHz and a coincidence window of 1 ns results in a 90% reduction in effective extraneous count rate.

intrinsic system electro-optical efficiency. This is determined by the transmit and receive aperture diameters, pointing accuracy, atmospheric absorption and turbulence, receiver internal losses, and detector efficiencies. We do not consider transmit telescope internal optical efficiency since WCP source intensities can be adjusted to maintain the desired average photon number at the exit aperture [34]. For each elevation, we also do not consider explicitly time-varying transmittance, since changes in channel losses are only due to changes in elevation with time. For discrete variable (DV) protocols, such as BB84, link efficiency fluctuations do not directly impact on the secret key rate, unlike in continuous variable (CV) QKD where this can appear as excess noise leading to a reduction in key [41, 42].

We have taken a simplified approach to the modelling of losses due to pointing and atmospheric effects. We base our link efficiency vs elevation values on concrete experimental measurements (see Extended data Fig. 3a in [43] and 3b for elevations 20° , 26° , 36° , and 55°) and construct a representative link efficiency with time curve extrapolating from 0° to 90° elevations or over the entire ± 350 s horizon to horizon passage time for a zenith overpass (Fig. 3). Link efficiency vs elevation curves are highly dependent on system performance and OGS site conditions, the Micius data should be regarded as a best-case scenario since the OGSS are situated in dark sky conditions at high altitudes of ~ 3000 m where the effects of atmospheric turbulence and attenuation are minimised. We also note that the link efficiency presented in [43] is for the entangled pair distribution experiments, not the prepare-measure QKD downlink system, but are still representative of the space-ground quantum channel link efficiencies that can be achieved with practical and current technologies.

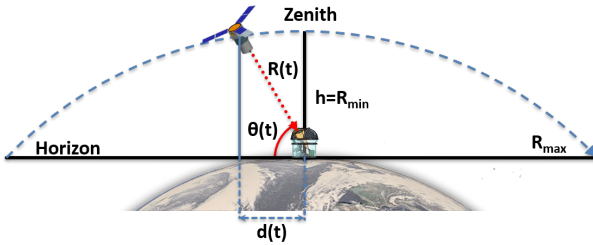


Figure 2. Illustration of a zenith pass. The simplest trajectory corresponds to when the ground track passes directly over the OGS position, hence the maximum elevation is 90° . This represents the ideal overpass with the maximum transmission time and lowest average channel loss. The elevation changes non-uniformly with time, with the greatest angular velocity at zenith of $0.87^\circ s^{-1}$ for $h = 500$ km and the satellite-OGS range $R(t)$ varies from 2600 km at the horizon to 500 km at zenith (14.32 dB change in far-field diffraction loss). The ground track distance from the OGS is denoted $d(t)$ and we take as $t = 0$ as the time of closest approach and maximum elevation θ_{\max} .

To allow formal comparison of our simulated results with different performing SatQKD systems, we introduce a system link efficiency $\eta_{\text{link}}^{\text{sys}}$. This parameterises the overall performance of the SatQKD system, which is specified as the link efficiency at zenith (Fig. 2). The nominal value for $\eta_{\text{link}}^{\text{sys}}$ considered is 27 dB, which corresponds to the improved Micius system using a 1.2 m diameter OGS receiver at Delingha. If smaller OGS receivers are used, or else there are greater constant losses, the per pass secret key length can be determined using worse (i.e. higher) plotted $\eta_{\text{link}}^{\text{sys}}$ values. We estimate the scaling of $\eta_{\text{link}}^{\text{sys}}$ with OGS aperture size straightforwardly. Under the assumption that the long term average ground spot size at minimum range is much larger than the OGS diameter D_r , we model the link efficiency change as $20 \log_{10}(D_r/D_r^0)$ (dB) where D_r^0 is the reference OGS diameter taken to be 1.2 m (Delingha OGS receiver diameter).

For changes to the transmitter aperture diameter, the time-averaged ground spot diameter may not be solely dominated by the far-field diffraction beam width. Specifically, contributions from the pointing performance and turbulence can also lead to significant additional beam broadening [44, 45]. The Micius mission reported sub- μ rad pointing performance and 10 μ rad beam widths from transmit apertures of 180 mm and 300 mm [43]. It is unclear the contribution of turbulence to the reported link efficiencies as a function of range/elevation. However it may be expected that the presence of non-diffractive beam spreading effects results in a smaller dependence of $\eta_{\text{link}}^{\text{sys}}$ on transmitter diameter D_t , i.e. using a smaller D_t should result in a smaller increase in $\eta_{\text{link}}^{\text{sys}}$ than given by purely diffractive beam broadening. As the focus of this paper is not a detailed analysis of atmospheric turbulence [46] or extinction [47], we refer the reader to alternative recent works, where the effects on satellite quantum communication are considered [39, 44, 48].

It should be noted that we can estimate the effect of increasing the source repetition rate by incorporating a correction factor to $\eta_{\text{link}}^{\text{sys}}$. As the secret key length is only a function of the total number of detection events per intensity level and

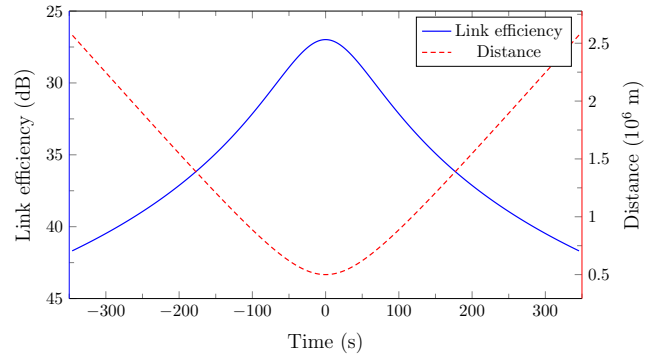


Figure 3. Loss vs elevation. Adapted from data in [43]. The link efficiency varies throughout the overpass due to the effects of changing range that leads to increased diffraction, and changes in elevation that alters the optical depth of the atmosphere and exposing the beam to varying turbulence effects. The peak $\eta_{\text{link}}^{\text{sys}} = 27$ dB occurs at zenith, which we call $\eta_{\text{link}}^{\text{sys}}$ to denote a characteristic system link performance level. We investigate different sized systems by adding a constant dB offset to the link efficiency curve to take into account different elevation independent losses such as a smaller or larger OGS receiver collection aperture or the use of detectors with a different photon detection efficiency.

the observed error rates, this only depends on the integrated product of the source rate and the link efficiency, keeping all other system parameters the same. Thus a 100 MHz source (as assumed in all simulations presented here) with a given $\eta_{\text{link}}^{\text{sys}}$ would provide the same amount of key as 1 GHz source with a 10 dB worse system link efficiency, e.g. with a 3 times smaller OGS receiver diameter.

We consider the quantum bit error rate (QBER) arising from dark counts, background light, source quality, basis misalignment, and receiver measurement fidelity. Again, we simplify our model by combining several of these together. The dark and background light count rates are assumed to be constant and independent of elevation (in practice background light will depend not just on elevation but also azimuth and the local environment). We combine all other error terms into an intrinsic quantum bit error rate QBER_I that does not vary with channel loss or elevation.

III. SATQKD OPERATIONS

A standard model of SatQKD has been the use of large, fixed, and long-term OGSs with which satellites regularly establish QKD links [26]. More demanding is where the OGS may only be able to communicate sporadically with a particular satellite and may not be able to accumulate sufficient data to process as a single large block. For example, smaller, mobile OGS terminals may be required to generate a key from a limited number of passes, possibly only one, due to operational constraints¹.

¹ We contrast this to fibre-based QKD, where the quantum channel is assumed to be stable (or can be made stable) and can be operated continuously until

It is common for the instantaneous (but asymptotic) key rate $R_\infty(t)$ to be calculated as a function of time during an overpass and integrated to arrive at the secret key length (SKL) [25, 26],

$$\text{SKL}_\infty^{\text{Cont.}} = \int_{t_{\text{start}}}^{t_{\text{end}}} R_\infty(t) dt, \quad (1)$$

where $t_{\text{start},\text{end}}$ define the start and end times of the quantum transmission period of the overpass. For a meaningful SKL, segments of data with the same statistical features from many passes are combined into an asymptotically large block for post-processing. In practice, small blocks from different passes are combined to give the following SKL,

$$\text{SKL}_\infty^{\text{Block}} = \sum_j R_\infty^j L_j, \quad (2)$$

where R_∞^j is the asymptotic key rate for a small segment j , and L_j its length. This restricts the operational flexibility and leads to considerable latency between the first contact between a satellite and an OGS and the generation of the first set of secret keys. A less restrictive mode of operation is to combine all data from several passes (without segmenting into similar sections of similar asymptotic rates) and process using asymptotically determined or assumed parameters, however the security promise of such a procedure would need to be closely examined.

Here, we consider a more flexible mode of operation whereby data from an overpass is processed as a single block taking into account finite length key statistics and uncertainties to maintain high levels of composable security (Fig. 4),

$$\text{SKL}_{\text{finite}} = \text{SKL} \left(\{n_k^\mu, m_k^\mu\} \right), \quad (3)$$

where $\{n_k^\mu, m_k^\mu\}$ are agglomerated count data without partitioning into sub-segments. This operational mode is considerably more practical for large constellations of satellites [25, 49] and number of OGSs where it would be resource intensive to keep track of and store a combinatorially large number of individual segmented link data until each had attained a sufficiently large block size for asymptotic key extraction. For these reasons, it is important to analyse the performance of SatQKD systems without assuming asymptotic key rates or infeasibly long operational periods to establish post-processing blocks.

IV. FINITE KEY LENGTH ANALYSIS

In this section, we determine the achievable finite key for different satellite passes using the optimised, decoy-state BB84 protocol with weak coherent pulses. Tight finite-key security bounds for this protocol have been derived for one [31] and two [30] decoy states. The difference between the use of one

a sufficiently large block size is collected. The minimum range, hence loss, can be made arbitrarily small thus high count rates and large block sizes, e.g. 10^{12} , are feasible.

and two-decoy state is small, however the use of two decoy states allows better estimation of the vacuum yield, which is important in the high loss regime. We optimise the two-decoy state protocol parameters and the amount of pass data to use in a block, accounting for practical constraints. This determines the average achievable key lengths that can be expected under different network operations. We also consider the sensitivity of the generated key length on different experimental parameters and satellite trajectories in order to derive a long term average amount of finite key.

The efficient BB84 protocol [50] encodes signals in X and Z bases with probabilities p_X and $1 - p_X$ respectively. It is a matter of convention which basis is used for key generation and the other for parameter estimation. In this work, the key is generated from X basis signals and the error rate in the Z basis is used to bound an eavesdroppers information on the raw key. The use of biased basis choice improves the sifting ratio without compromising the security. In the asymptotic regime, the sifting ratio tends to 1, compared with 0.5 for symmetric basis choice as in the original formulation of BB84. As we demonstrate later in section IV E, this sifting ratio advantage persists in the finite key regime, leading to longer raw sifted key for a given number of transmitted signals. This reduces parameter estimation uncertainties as well as provides more distillable raw key in the first place. The key is generated only from events corresponding to cases where the two authorised parties choose the X basis, and its phase error rate is determined from joint Z basis choices.

Practical BB84 implementations generally use phase-randomised laser-generated weak coherent pulses (WCPs) instead of true single photon sources as the latter devices are currently unavailable for field deployment [51]. Phase randomised WCPs are a probabilistic mixture of photon number (Fock) states, even weak pulses will have a non-trivial fraction of multi-photon emissions. Pulses that contain two or more photons compromise the security of basic BB84 due to the possibility of photon number splitting (PNS) attacks unless the channel loss is kept relatively low [52]. So-called decoy state methods were proposed as a method to detect PNS attacks and have rapidly become the *de facto* method of implementing prepare and measure QKD using WCP sources [6].

For the three-intensity (or two-decoy state) BB84 protocol, the sender chooses to send one of three intensities μ_j for $j \in \{1, 2, 3\}$ with probabilities p_j . For the purposes of the security proof, we assume that $\mu_3 = 0$ is the vacuum state, and the other intensities satisfy $\mu_1 > \mu_2$ and $\mu_2 > 0$. The finite key attainable with two decoy states is given by [30],

$$\ell = \left\lfloor s_{X,0} + s_{X,1}(1 - h(\phi_X)) - \lambda_{\text{EC}} - 6 \log_2 \frac{21}{\epsilon_s} - \log_2 \frac{2}{\epsilon_c} \right\rfloor, \quad (4)$$

where $s_{X,0}$, $s_{X,1}$ and ϕ_X , are the vacuum yield, single-photon yield, and the phase error rate associated with the single-photon events respectively. For a satellite, unlike in the fibre case considered in [30], one cannot fix the size of the sifted X-basis data block. Instead, we have a fixed number of pulses, N , sent per pass. This number is determined by the laser rep-

Algorithm 1 $\{\eta_{\text{link}}^{\text{sys}}(j), \ell[j], \text{QBER}\} = \text{OPTIMISED SKL } (N, M, L)$

```

1:  $C_1 \leftarrow 0 < p_X < 1$ 
2:  $C_{2,3,4} \leftarrow 0 < p_j < 1$  for  $j = 1, 2, 3$ 
3:  $C_{5,6} \leftarrow 0 < \mu_j < 1$  for  $j = 1, 2$ 
4:  $C_7 \leftarrow \mu_1 - \mu_3 > \mu_2$ 
5:  $C_8 \leftarrow \mu_2 > \mu_3$ 
6:  $N \leftarrow$  number of pulses per second
7:  $M \leftarrow$  number of satellite passes
8:  $L_t \leftarrow$  elevation dependent loss at time  $t$ 
9:  $t_0 \leftarrow$  time at max elevation
10:  $\tau_n \leftarrow$  probability of  $n$ -photon transmission
11:  $\mathbf{v} \leftarrow \mathbf{0}$ 
12: for all  $j = 0$  to 15 dB do
13:   for all  $\Delta t = 0$  to  $t_{\text{max}}$  do
14:      $\eta_{\text{link}}^{\text{sys}}(j) \leftarrow L_{t_0} + l_{s_j}$ 
15:      $[D(j)]_{kl} \leftarrow$  detection probability of pulse  $k$  at time  $l$ 
16:      $[E(j)]_{kl} \leftarrow$  error probability of pulse  $k$  at time  $l$ 

—Generate data (error) block sizes for pulse  $k$ —
17:      $[n_{X(Z)}]_k \leftarrow \sum_{l=t_0-\Delta t}^{t_0+\Delta t} N p_k p_{X(Z)}^2 [D(j)]_{kl}$ 
18:      $n_{X(Z),k}^{\pm} \leftarrow [n_{x(z)}]_k \pm \delta_{X(Z),k}^{\pm}$ 
19:      $n_{X(Z)} \leftarrow \sum_k [n_{x(z)}]_k$ 
20:      $s_{x,0} \leftarrow \tau_0 \frac{\mu_2 n_{x,3} - \mu_3 n_{x,2}}{\mu_2 - \mu_3}$ 
21:      $s_{x,1} \leftarrow \frac{\tau_1 \mu_1 \left[ n_{x,2} - n_{x,3} - \frac{\mu_2^2 - \mu_3^2}{\mu_1^2} \left( n_{x,1}^+ - \frac{s_{x,0}}{\tau_0} \right) \right]}{\mu_1 (\mu_2 - \mu_3) - \mu_2^2 + \mu_3^2}$ 
22:      $\phi_X \leftarrow$  phase error rate
23:      $\ell[j, \Delta t] \leftarrow \frac{1}{M} \left[ s_{x,0} + s_{x,1} (1 - h(\phi_X)) - \lambda_{\text{EC}} - 6 \log_2 \frac{21}{\epsilon_a} - 6 \log_2 \frac{2}{\epsilon_c} \right]$ 
24:     Maximize  $\ell[j, \Delta t]$  over constraints  $\{C_1, \dots, C_8\}$ 
25:      $v_j \leftarrow \{\eta_{\text{link}}^{\text{sys}}(j), \sup_{\Delta t} \ell[j, \Delta t], \text{QBER}\}$ 
26: Return  $\mathbf{v}$ 

```

Figure 4. Pseudocode to determine the optimised finite key length for a satellite pass. The optimisation is performed over all protocol parameters and the transmission time window Δt over which raw key is acquired. The correction terms $\delta_{X(Z),k}^{\pm}$ for the bases $X(Z)$ and the intensities μ_k come from the multiplicative Chernoff bound that accounts for finite statistics [33].

etition rate and the fraction of the orbit from which we collect data. The sizes of the X and Z basis data blocks are calculated from N , the probability of detecting a pulse (which is function of time), and the sifting ratios. Next, we look into the security conditions of this secret key.

For error correction, error syndrome information is exchanged over a public channel to correct key strings. The number of bits leaked during error correction is denoted λ_{EC} , and is accounted for during privacy amplification. In the finite key regime, this information leakage has a fundamental upper bound $\lambda_{\text{EC}} < \log |\mathcal{M}|$, where \mathcal{M} characterises the set of syndromes in the information reconciliation [32]. We use an estimate of λ_{EC} that varies with block size [32] (details in Appendix A).

The security of the key rate for the decoy state efficient BB84 protocol is defined via the following statement: For small security parameters, $\epsilon_c, \epsilon_s > 0$, the protocol is $\epsilon = \epsilon_c + \epsilon_s$ -secure if it is ϵ_c -correct and ϵ_s -secret [30, 53]. For numerical optimisation, we take $\epsilon_c = 10^{-15}$ and $\epsilon_s = 10^{-9}$. Conditioned on passing the checks in the error-estimation and error-verification steps, an ϵ_s -secret key of length ℓ can be attained.

We implement a numerical optimiser to determine the achievable secret key length for a satellite pass, illustrated by pseudocode in Fig. 4, using improved finite key analysis

to that in Ref. [30]. The main difference, is in estimating the terms $\delta_{X(Z),k}^{\pm}$, which are corrections due to the finite statistics. Instead of using the Hoeffding bound, we employ the tighter, multiplicative Chernoff bound [33], to estimate $\delta_{X(Z),k}^{\pm}$ (see Appendix A). In the following, we provide a detailed analysis of how different factors, such as system parameters and pass geometry, influence the achievable finite key length.

A. Transmission time window optimisation

After the quantum transmission phase of an overpass (or several), we group together the sifted raw key to process in a single block. In addition to optimising the protocol parameters, we can also optimise the over elevations over which we include data in the processing block, i.e. trimming data from the start and end of the overpass to produce a truncated block. For small elevation angles (around the horizon), the high losses mean that the signal count rate is lower and a relatively higher proportion of extraneous counts when compared to larger elevation angles (where the satellite passes nearer to zenith). The QBER is thus greater at lower elevation angles than at higher angles. Excluding data from the start and end of the overpass results in a lower average QBER for the raw key. The reduction in QBER, however, comes at a cost of reducing the length of the raw key. This unveils a trade-off between length of raw key and QBER. This trade-off necessitates an optimisation of the protocol parameters (biased probabilities and intensities) *and* the length of each transmission window over which the finite key is assimilated.

For any satellite pass, we define $t = 0$ as the time where the satellite reaches maximum elevation, and $\pm t_{\text{max}}$ as the time at which the satellite is at local horizon, i.e. where the elevation angle is zero. We consider a transmission window, Δt ($0 < \Delta t \leq t_{\text{max}}$) over which data is collected into a raw key block. We assume that the transmission window extends from $-\Delta t$ to $+\Delta t$, i.e. the region surrounding maximum elevation. For intermediate values of Δt , a partial satellite trajectory path is used to construct a finite key. Fig. 5 shows for different $\eta_{\text{link}}^{\text{sys}}$ the achievable secret key length (SKL) for varying values of Δt , hence data used, for a zenith pass.

We observe that for systems with good $\eta_{\text{link}}^{\text{sys}}$, the QBER at low elevations does not rise greatly above QBER_1 . As such, it is generally better to keep more data by keeping Δt close to t_{max} . For poor $\eta_{\text{link}}^{\text{sys}}$, however, restricting the elevations over which data is included to near zenith can lead to a longer SKL (see Fig. [28], $\eta_{\text{link}}^{\text{sys}} = 35$ dB). This is due to the improvement in error rate counteracting the smaller raw key length and slightly larger uncertainties due to a smaller sample size.

Our values of QBER are calculated for a whole pass, and thus represent an average of the instantaneous QBER. Nevertheless, the values presented in Fig. 5 are consistent with the instantaneous QBERs found in the Micius satellite [28].

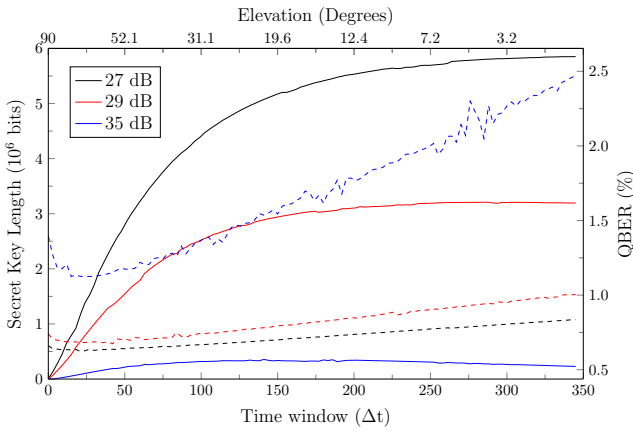


Figure 5. Secret key length and QBER vs zenith pass segment size. Solid lines are for different $\eta_{\text{link}}^{\text{sys}}$ and dashed lines represent corresponding truncated block QBERs. System parameters are $\text{QBER}_I = 0.5\%$ and $p_{\text{ec}} = 10^{-6}$. For each Δt , the protocol parameters were optimised for maximum SKL using data in the interval $-\Delta t$ to $+\Delta t$. Increasing Δt to large values only leads to minor increases in the SKL. For example restricting a $\eta_{\text{link}}^{\text{sys}} = 27$ dB system to $-150s \leq t \leq +150s$ instead of the full $\pm 350s$ leads to only a $\sim 10\%$ drop in SKL and using only $-50s \leq t \leq +50s$ achieves 50% of the maximum SKL for a single pass. For worse $\eta_{\text{link}}^{\text{sys}}$, inclusion of data from low elevations is detrimental since they have high error rates due to low signal to noise (SNR). This contaminates the data from around zenith that have higher raw count rates, higher SNR and thus much lower QBER. Satellite passes around the horizon yield large error rates, this is seen in the rise of the truncated block QBER, especially for $\eta_{\text{link}}^{\text{sys}} = 35$ dB where increasing the transmission window into the low elevation region degrades the total SKL. Although our QBER is for the whole pass, and thus represents an average, the values are nevertheless consistent with the QBER found in the Micius satellite [28]. Numerical instabilities in the QBER for $\eta_{\text{link}}^{\text{sys}} = 35$ dB appear since it is not the objective function of the optimisation program.

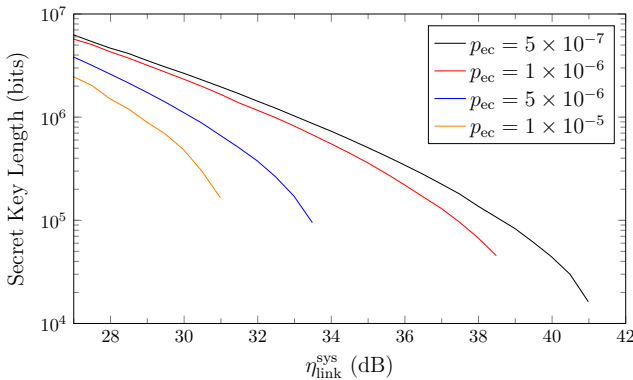


Figure 6. SKL with link efficiency for different extraneous count rates. Solid lines represent the finite key attainable with a single satellite pass over zenith, while dashed lines represent the finite key, per pass, for two passes. For each curve, QBER_I is 0.5% and the after pulse probability 0.1% . We consider 20% additional extraneous count rates over the baseline considered by Micius, which could represent operation near a full Moon or severe light pollution.

B. SKL dependence on system parameters

In this section, we determine the dependence of the optimised finite key length to different system parameters: extraneous counts (detector dark count and background light); and intrinsic quantum bit errors QBER_I . For each analysis, we optimise over all protocol parameters in addition to the satellite transmission window. The achievable SKL is then determined for different $\eta_{\text{link}}^{\text{sys}}$ representing differently performing SatQKD systems, e.g. using smaller OGS diameters, that introduce additional losses (independent of elevation) over the reference system with $\eta_{\text{link}}^{\text{sys}} = 27$ dB. We denote changes to $\eta_{\text{link}}^{\text{sys}}$ by adding η_{excess} such that $\eta_{\text{excess}} = 10^{(-l_s/10)}$, where l_s is the corresponding difference in $\eta_{\text{link}}^{\text{sys}}$ in dB.

We consider η_{excess} up to 15 dB (corresponding to $\eta_{\text{link}}^{\text{sys}} = 42$ dB) equivalent to using a $D_r = 21.3$ cm diameter OGS instead of the reference $D_r = 1.2$ m, keeping all other system parameters unchanged unchanged. Notably we only consider worse total link efficiencies than the concrete nominal system loss demonstrated by the Micius satellite-OGS link. Negative η_{excess} , corresponding to the use of more efficient detectors or larger OGSs, would result in an increase in the attainable key.

We first consider the effects of different extraneous count rates p_{ec} on the achievable key lengths (Fig. 6). For OGS receivers, the constraints on detector size, weight, and power (SWaP) are not as severe as for space-based detectors, however it is desirable to reduce the cost and complexity of such systems. Although superconducting nanowire single photon detectors exhibit excellent photon detection efficiency with improved quantum efficiencies across a wide range of wavelengths with very low jitter and dark count rates [54], the need for cryogenic coolers and single mode coupling (necessitating the use of adaptive optics) greatly restricts widespread deployment. Silicon SPADs are the preferred option for Vis/NIR photons with moderately high PDE and sufficiently low dark count rate with conventional thermoelectric cooling of the order of 10s of counts per second, leading to a few error counts per second taking into account temporal filtering [55].

In typical OGS environments (i.e. not under dark sky conditions), we can assume that background light will be a significant contribution to the extraneous count rate. In our analysis, we account for stray light from celestial bodies and human activity adding to the detector dark count which is lumped together into a single extraneous count rate. Notice, that the extraneous count rate has a significant impact on the SKL. While it can increase the vacuum yield this effect is more than compensated by the increase in ϕ_X and λ_{EC} . The net effect is to decrease the SKL. Specifically, a factor of 10 increase in the p_{ec} reduces the achievable SKL by 40% at 27 dB. Further, the effects of extraneous counts are compounded by increased loss. In particular, in the high loss regime, an increase in extraneous count can result in no finite key being generated. This indicates that extraneous counts have a strong influence on the QBER, when $\eta_{\text{link}}^{\text{sys}}$ becomes worse.

We now look at the effect of intrinsic errors, e.g. due to a less than unit fidelity of the source states, misalignment of the satellite and receiver reference frames, or non-ideal projective measurements by the OGS (Fig. 7). We lump all these effects

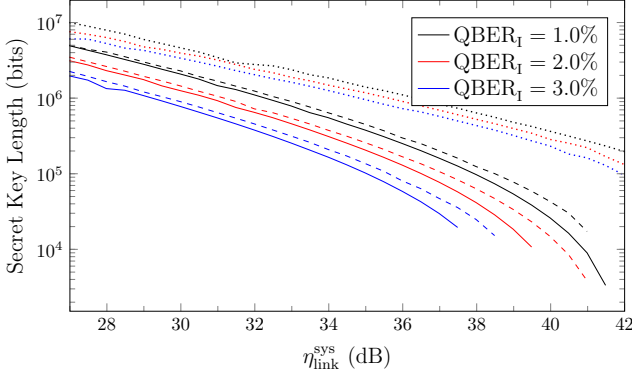


Figure 7. SKL with link efficiency for different values of QBER_I . Solid lines represent the finite key attainable with a single satellite pass over zenith, while dashed lines represent the normalised (per pass) finite key, using combined data from two passes. The dotted lines represent the normalised block asymptotic SKL (Sect. IV D). The extraneous count rate is $p_{\text{ec}} = 5 \times 10^{-7}$ per pulse and the after pulse probability 0.1%.

into a quantity QBER_I that characterises the intrinsic error of the system that is independent of the count rate. We observe that the finite key length is not as susceptible to changes in the QBER_I as compared with p_{ec} .

Other factors affecting the SKL include signal intensities μ_j , their probabilities p_j , and basis bias p_X . The optimised values of these system parameters generally depend on the excess loss considered. Fig. 8 shows how the optimised protocol parameters change with the total link efficiency. We see that as $\eta_{\text{link}}^{\text{sys}}$ increases (worsens), p_X decreases meaning that Alice needs to send more pulses in the Z basis. This comes from the fact that as the loss increases, the OGS detects fewer photons leading to worse parameter estimation of $s_{X,0}$, $s_{X,1}$ and ϕ_X from fewer statistics. To compensate, we need to collect more Z basis events by increasing p_Z i.e. by decreasing p_X . The reduced number of key generation events (X basis detections) is outweighed by better bounds on the key length parameters. This implies that the uncertainties in the parameter estimation from finite statistics dominates the SKL compared with raw key length when $\eta_{\text{link}}^{\text{sys}}$ becomes poor.

C. Non-zenith passes

The typical pass will not pass over zenith, hence it is necessary to analyse the SKL achievable from non-ideal overpasses (Fig. 1). Here, we explore the effect of $\eta_{\text{link}}^{\text{sys}}$ on the lowest elevation pass θ_{max}^- that still results in non-zero finite key and how this affects the long-term average SKL. In Fig. 9 we illustrate the achievable SKL depending on the minimum zenith angle $\alpha_{\text{min}} = 90^\circ - \theta_{\text{max}}^-$ attained during the pass. As expected larger minimum zenith angles α_{min} leads to smaller SKL due to shorter transmission times as well as lower count rates due to worse average η_{link} at lower elevations and longer ranges. The SKL vanishes when the satellite pass is above a critical zenith angle α_{min}^+ . This is a crucial point for any QKD satellite

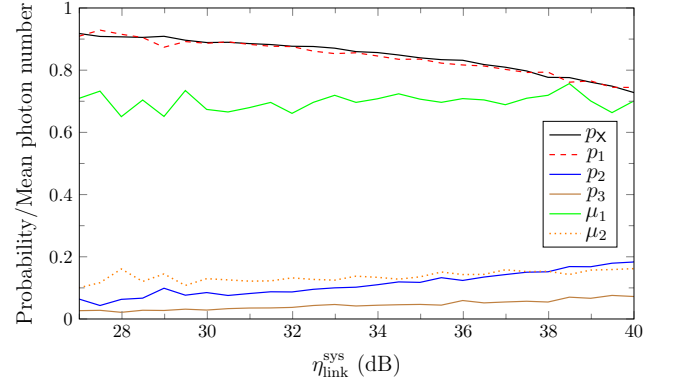


Figure 8. Optimisation parameters vs $\eta_{\text{link}}^{\text{sys}}$ for zenith pass. System parameters are $p_{\text{ec}} = 5 \times 10^{-7}$ and QBER_I of 0.5%.

mission design as we can only extract a finite key for satellite passes that yield sufficient data.

In order to estimate the average amount of secret key that can be generated with single pass blocks, we first integrate the area under the SKL vs d_{min} curve,

$$\text{SKL}_{\text{int}} = 2 \int_0^{d_{\text{min}}^+} \text{SKL}_{d_{\text{min}}} dd_{\text{min}}, \quad (5)$$

where d_{min}^+ is the maximum OGS ground track offset that results in finite key (see Fig. 9). We can then estimate the annual average key (in the absence of weather effects and variation of p_{ec} , e.g. due to time of year, phase of Moon) by,

$$\overline{\text{SKL}}_{\text{year}} = N_{\text{orbits}}^{\text{year}} \frac{\text{SKL}_{\text{int}}}{L_{\text{lat}}}, \quad (6)$$

where $N_{\text{orbits}}^{\text{year}}$ is the number of orbits of the satellite per year, and L_{lat} is the longitudinal circumference at the latitude of the OGS. This assumes that, on average, d_{min} is evenly distributed (unless in an Earth synchronous orbit [25]) and that the OGS is at low to moderate latitudes as the approximation becomes worse at the poles due to the orbital inclination ($\sim 97^\circ$) of an SSO orbit. For $h = 500$ km, $N_{\text{orbits}}^{\text{year}} \sim 5500$ and the circumference along a line of longitude at the position of Glasgow (55.9° N) is $L_{55^\circ} \sim 2.25 \times 10^7$ m resulting in $\overline{\text{SKL}}_{\text{year}} = 2.44 \times 10^{-4} \text{SKL}_{\text{int}}$.

D. Multiple satellite passes

We now explore how combining separate satellite passes can improve secret key lengths for situations where some degree of key generation latency can be tolerated and the single-pass finite key assumption can be relaxed. Fig. 7 illustrates the finite and asymptotic secret key-lengths for a single zenith satellite pass. The asymptotic key rate corresponds to many satellite passes where the block sizes used to determine the key rate tend to infinity. Note that we do not use the process given by Eq. 2, instead we put together all the data from the passes into a single block for processing and do not use

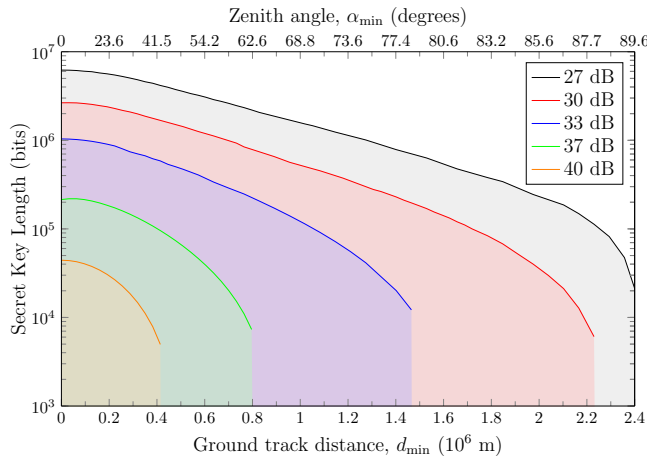


Figure 9. SKL vs ground track offset. We plot the finite key length attainable with varying minimum ground track distances between the satellite and OGS for different $\eta_{\text{link}}^{\text{sys}}$. The system parameters were $p_{\text{ec}} = 5 \times 10^{-7}$ and $\text{QBER}_1 = 0.5\%$. The key generation footprint is given by the maximum d_{min} that still results in non-zero finite key. The maximum footprint is limited by visibility above the horizon, for $h = 500$ km the maximum total width is 4887 km. Here, we have assumed that quantum transmission can occur horizon to horizon. In practice, quantum transmission may not be possible immediately after the satellite rises above the horizon due to the need for initiation and stabilisation of tracking, handshake protocols, and local skyline obstructions. Similarly, as the satellite sets the quantum transmission may need to terminate before θ reaches 0° to allow for post-processing and finalisation of all reconciliation steps. If we assume a non-zero minimum elevation below which quantum transmission does not occur, this would decrease α_{min}^+ and move all the curves down. It may be reasonable to set $\alpha_{\text{max}}^+ = 80^\circ$ for advanced SatQKD systems leading to a maximum key generation footprint of 3200 km total width ($d_{\text{min}}^+ = 1600$ km).

System loss	SKL _{int}	SKL _{55°N}
27 dB	9.22×10^{12} bm	2.2536 Gb
30 dB	3.52×10^{12} bm	0.8603 Gb
33 dB	1.12×10^{12} bm	0.2740 Gb
37 dB	1.76×10^{11} bm	0.0429 Gb
40 dB	2.28×10^{10} bm	0.0056 Gb

Table II. Expected yearly average secret finite key lengths attainable for different satellite trajectories. The quoted SKL_{int} correspond to the integrated area under each SKL vs ground track distance curve in Fig. 9 and is in units of bit-metres (bm). We have not included weather effects or considered a minimum elevation for quantum transmission so these values should be considered an optimistic upper bound.

a segmented or instantaneous asymptotic key rate; we only assume that the aggregated block parameters are known with negligible uncertainty. The process of taking the block size to infinity requires care for satellites, as each orbit yields a fixed amount of data. A detailed discussion of the asymptotic limit is given in Appendix C. As expected, the key length increases significantly if the block asymptotic regime can be reached.

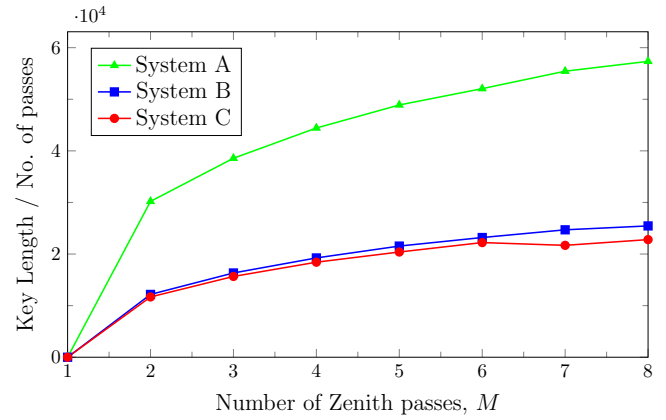


Figure 10. Plot of normalised (per pass) SKL vs number of passes. The plot shows the SKL achievable by combining data from multiple zenith passes before processing as a single block. The different curves correspond to different sets of system parameters with different $\{\eta_{\text{link}}^{\text{sys}}, p_{\text{ec}}, \text{QBER}_1\}$: A={45.7 dB, 10^{-7} , 0.5%}, B={44.8 dB, 10^{-7} , 1%}, and C={40.5 dB, 5×10^{-7} , 1%}.

Generating key from a single pass constrains the achievable secret key length. One way to approach the asymptotic key rate is to accumulate more signals through multiple satellite passes. This approach assumes that latency in key generation and the storage of raw key can be tolerated. Fig. 10 illustrates the improvement from multiple zenith passes where non-zero finite key cannot be generated in a single zenith pass for different combinations of system parameters. The relative improvement depends on the system link efficiency. The origin of this improvement is purely due to smaller parameter estimation uncertainties owing to increased statistics since averaging over several pass does not improve the actual QBER or phase error (ϕ_X) rates, though is a small improvement due to better error correction efficiency and reduced λ_{EC} . This clearly illustrates the principle difficulty in satellite QKD; fluctuations in finite statistics severely limit the average attainable SKL.

Combining the data from multiple passes can improve the key length per pass. In particular, we can obtain non-zero key when $\eta_{\text{link}}^{\text{sys}}$ is too poor for key generation from a single pass. However, this must be balanced against greater key generation latency and potential security issues from needing to store large amounts of raw data for a longer period of time between passes. Ensuring the security of the OGS for several passes is more difficult than ensuring its integrity over a single pass. We assume that key is consumed soon after generation so the attack horizon is dominated by the period in which secret data is at rest.

E. Protocol Selection

To illustrate the effect of statistic uncertainties in constraining the key length under finite block size assumptions, we compare the performance of two variants of BB84: efficient BB84 (as considered thus far) [50] and standard BB84 [56]. The main difference is in the choice of bases, standard BB84 chooses

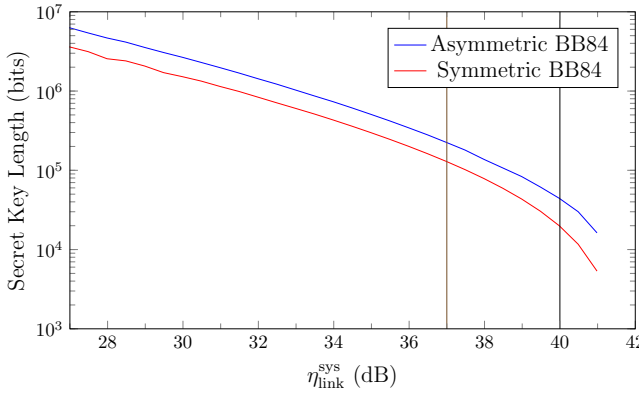


Figure 11. SKL vs $\eta_{\text{link}}^{\text{sys}}$ for asymmetric and symmetric BB84 protocols. System parameters are $p_{\text{ec}} = 5 \times 10^{-7}$, and $\text{QBER}_I = 0.5\%$. The vertical lines at $\eta_{\text{link}}^{\text{sys}} = 37$ dB and 40 dB indicates the system configurations for which we explore the elevation dependence of both protocols in Fig. 12.

both X and Z bases with equal (symmetric) probability whilst efficient BB84 is allowed to favour one basis over the other (asymmetric basis choice). standard BB84 also uses both bases to generate key and perform parameter estimation, whilst efficient BB84 uses only one basis for key generation whilst the other is only used solely for parameter estimation. Due to these differences, we will refer to the two protocols as symmetric and asymmetric BB84 respectively.

Fig. 11 illustrates the attainable key length for a single satellite pass over zenith with varying levels of system link efficiency in the link efficiency. Notice that the asymmetric protocol achieves both a better key length for all values of system link efficiency. Fig. 12 shows the SKL as a function of maximum zenith angle for non-zenith passes and shows that the asymmetric protocol generates more keys for all satellite trajectories. This amounts to an increased average key generation per year of 86% and 180% for $\eta_{\text{link}}^{\text{sys}} = 37$ dB and $\eta_{\text{link}}^{\text{sys}} = 40$ dB respectively under the most generous assumptions (no weather or minimum elevation effects).

The advantages of the asymmetric protocol stem from several factors. Firstly, the asymmetric protocol retains more raw bits at the sifting stage. This obviously leads to a larger final secret key. However, retaining more of the raw key bits also allows us to perform better parameter estimation. This is a crucial advantage for finite-key QKD. As we have seen, finite key analysis is extremely sensitive to how well we estimate the parameters. In particular, a small increase in loss can result in the key length dropping to zero.

The next advantage of the asymmetric protocol is more subtle. In asymmetric BB84, we use all the Z-basis events to estimate the vacuum and single photon yields. In contrast, for symmetric BB84, we reveal a random sub-sample of results for *each* basis, where each amount is optimised. The vacuum and single photon yields for the X or Z bases are found using only results corresponding to that basis. This means that only *half* of the revealed results are used to estimate the yields for each basis. In contrast, in the asymmetric protocol, *all* of the revealed results are used to estimate the yields.

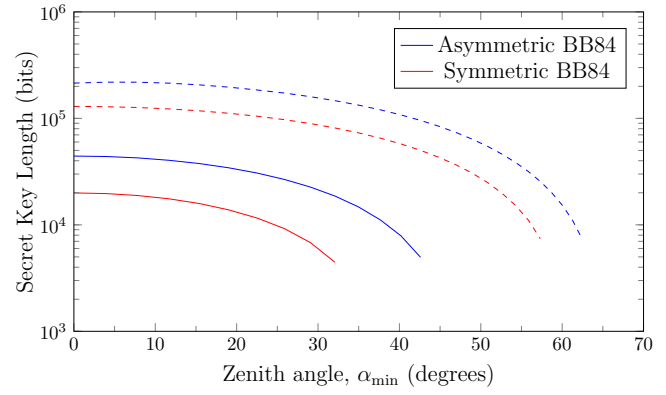


Figure 12. Plot of key length (in bits) attainable using the asymmetric and symmetric BB84 protocols with varying max altitude satellite elevation angles. Solid lines correspond to a system link efficiency of $\eta_{\text{link}}^{\text{sys}} = 40$ dB, and dashed lines with $\eta_{\text{link}}^{\text{sys}} = 37$ dB, both with $p_{\text{ec}} = 5 \times 10^{-7}$, $\text{QBER}_I = 0.5\%$. As in Sec. IV C, we can calculate SKL_{int} and SKL_{year} to arrive at $\{1.76 \times 10^{11} \text{ bm}, 42.9 \text{ Mb}\}$ and $\{9.43 \times 10^{10} \text{ bm}, 23.0 \text{ Mb}\}$ for $\eta_{\text{link}}^{\text{sys}} = 37$ dB, and $\{2.28 \times 10^{10} \text{ bm}, 5.58 \text{ Mb}\}$ and $\{8.14 \times 10^9 \text{ bm}, 1.99 \text{ Mb}\}$ for $\eta_{\text{link}}^{\text{sys}} = 40$ dB for the asymmetric and symmetric protocols respectively. The inefficiency of symmetric BB84 is apparent, asymmetric BB4 is able to generate $1.86 \times$ and $2.80 \times$ more key on average for $\eta_{\text{link}}^{\text{sys}} = 37$ dB and $\eta_{\text{link}}^{\text{sys}} = 40$ dB respectively. The advantage is seen to grow as $\eta_{\text{link}}^{\text{sys}}$ become worse. If minimum elevation limits for quantum transmission is considered, the relative advantage can only increase.

One final advantage is that asymmetric BB84 requires less classical communication. In particular, we do not need to communicate the choice of which bits to reveal to estimate the QBER and other parameters. Instead, this task is achieved by the choice of basis. One slight disadvantage of asymmetric BB84 is in the biased basis choices. A quantum random number generator needs to generate several unbiased bits to produce a single biased bit (at worst 2 unbiased bits per biased bit on average using a non-deterministic algorithm). However, after this stage, the storage requirements for these basis bits is identical in both symmetric and asymmetric BB84.

This analysis shows that in the finite key regime, asymmetric BB84 is both more efficient and practical than symmetric BB84. It is able to deliver improved key rates for a wider range of system parameters and system link efficiencies. Additionally, it can provide a non-zero key for more orbits than symmetric BB84.

V. CONCLUSIONS AND DISCUSSIONS

We have analysed how the attainable secret key length varies with a single or multiple overpasses under the finite key block size assumption. This type of analysis is important for establishing the security of realistic operational models for practical SatQKD. Our study explores the influence of different parameters, including: the system link efficiency performance level characterised by $\eta_{\text{link}}^{\text{sys}}$, intrinsic source and measurement

quality characterised by QBER_1 , extraneous count rate including detector dark counts and background light with combined probability p_{ec} per pulse, pass geometry, and raw data block length. We use as the basis for $\eta_{\text{link}}^{\text{sys}}$ the most recent data from the Micius satellite as representative of the current state of the art performance.

We show that extraneous count rates are more detrimental than worse intrinsic QBER to the finite size secret key length due to the effect of worse link efficiencies at low elevations affecting the raw key error rates. We find that only a few passes are required to raise zero finite SKL to positive values quickly approaching asymptotic rates. Small efficiency gains can lead to large average SKL amounts due to the expanded key generation footprint enabled. This can be seen in the SKL_{year} averages that shows a large dependence on $\eta_{\text{link}}^{\text{sys}}$. For example, for the nominal system parameters, a change from $\eta_{\text{link}}^{\text{sys}} = 37$ dB to $\eta_{\text{link}}^{\text{sys}} = 40$ dB (factor of 2) results in a $7.7 \times$ reduction in the yearly average rate since not only is the SKL for a given θ_{max} reduced, the key generation footprint, compounding the reduction.

Further work could include more general loss vs elevation models so that more diverse systems and OGS locations can be studied. Operational constraints on the transmission time may impact on achievable key rates for poor $\eta_{\text{link}}^{\text{sys}}$ at low elevations and requires further study. For example if post-processing and all reconciliations steps need to be completed before the end of the overpass, this will introduce a minimum gap between the end of the quantum transmission and the time the satellite passes below the horizon that will impact upon SKL and θ_{max}^- . The effect of source rate is implicit in the analysis via a change of $\eta_{\text{link}}^{\text{sys}}$ axis origin as previously discussed. Our model can be combined with higher fidelity orbital and constellation modelling for more precise long term average SKL prediction, taking into account local atmospheric and weather conditions [25, 49]. We can also extend our finite key analysis to other protocols, such as CV-QKD with appropriate modification of the SKL and optimisation procedures.

ACKNOWLEDGMENTS

We acknowledge support from the UK NQTP and the Quantum Technology Hub in Quantum Communications (EPSRC Grant Ref: EP/T001011/1), the UK Space Agency (NSTP3-FT-063, NSTP3-FT2-065, NSIP ROKS Payload Flight Model), the Innovate UK project ReFQ (Project number: 78161), and QTSPACE (COST CA15220). DO is an EPSRC Researchers in Residence at the Satellite Applications Catapult (EPSRC Grant Ref: EP/T517288/1). DO and TB acknowledge support from the Innovate UK project AirQKD (Application number: 45364). DO and DM acknowledge support from the Innovate UK project ViSatQT (Project number: 43037). RP acknowledge support from the EPSRC Research Excellence Award (REA) Studentship. The authors thank J. Rarity, D. Lowndes, S. K. Joshi, E. Hastings, P. Zhang, and L. Mazzarella. for insightful discussions. DO also acknowledges discussion with S. Mohapatra, Craft Prospect Ltd., and support from the EPSRC Impact Acceleration Account.

Appendix A: Finite key analysis for decoy-state BB84

The Bennett–Brassard 1984 (BB84) quantum key distribution (QKD) protocol has become widely implemented owing to its simplicity, overall performance and provable security [56]. Practical implementations, however, depart from the idealised single-photon sources required in the original theoretical proposal. Instead, weak pulsed laser sources are used due to availability and ease of implementation compared with true single photon sources. While this delivers improved repetition rates over current single photon sources, the unmodified BB84 protocol is vulnerable to photon-number-splitting (PNS) attacks that exploit multi-photon pulse fraction present in each weak coherent pulse signal [57].

To overcome PNS attacks and extend the range of WCP sources, the so-called decoy-state protocols were developed. These employ multiple Poisson photon number distributions associated with different phase randomised coherent state intensities that allow more accurate characterisation of the photon number distribution of the transmitted pulses associated with detection events [58]. In this way, the secure fraction of the sifted raw key (vacuum and single photon yields) can be reliably estimated, which makes the decoy-state BB84 protocol a secure and practical implementation of QKD².

The security of decoy-state QKD was initially developed assuming the asymptotic-key regime [59, 60]. Such an analysis neglects fluctuations due to finite statistics. To compensate, security analyses for finite-length keys have been developed [61–63]. However, early approaches used a Gaussian assumption to bound the difference between the asymptotic and finite results. As such, their validity is restricted to collective attacks, rather general coherent attacks. Security analyses for general attacks have also been developed [64]. The multiplicative Chernoff bound [36, 65] and Hoeffding inequality [30] can be used to bound the fluctuations between the observed values and the true expectation value. A more complete finite-key analysis for decoy-state based BB84, with composable security, has recently been presented in [33]. This uses the multiplicative Chernoff bound, and presents simple analytic expressions, which are still reasonably tight.

The approach we adopt is a modification of [30]. We use the same structure but replace the Hoeffding bound with the inverse multiplicative Chernoff bound, as proposed in [33, 65], specifically, using equations (9) and (10) of [33] to obtain new expressions for the finite statistical corrections terms, $\delta_{X(Z),k}^\pm$, that appear in equations (2)–(4) of [30].

² Though the term “decoy state” has been used to describe such protocols, it is a slight misnomer when applied to current protocols. The original idea was to use decoy states of differing intensities to identify the presence of an eavesdropper performing PNS attacks, the results of the decoy states were discarded and only the detection event corresponding to “signal”; states were used for the final key. However, it is not only possible but also more efficient to utilise all intensity pulses to derive the final key, hence they can all be considered as “signal”. In light of this, it may be more accurate to describe such protocols as “multi-intensity” WCP QKD and relegate the term “decoy” as a historical footnote. But to maintain consistency with historical usage, we will continue to refer to these protocols as “decoy-state”.

An important step in any QKD protocol is error correction. This necessitates classical communication, of λ_{EC} bits, which are known to Eve. This must be taken account of in the privacy amplification stage.

In an actual run of the protocol, one would know λ_{EC} , however, for optimisation, we must estimate it. If this estimate is too pessimistic, then we could conclude that no key can be extracted in a region where one is still viable. Conversely, an overly optimistic value for λ_{EC} can lead to spurious results.

It is standard to model the channel as a bit-flip channel. This leads to $\lambda_{EC} = f_{EC}n_Xh_2(Q)$, where Q is the QBER and f_{EC} is the reconciliation factor. The value of f_{EC} is typically slightly above 1, e.g. 1.16. The use of a constant reconciliation factor is a simple way of accounting for inefficiency in the error correction protocol. This approach is normally sufficient when determining the optimal secret key length. However, for satellite QKD, one operates with high losses that are at the limit of where one can extract a key. As such, it is beneficial to use a more refined estimate of λ_{EC} .

A better estimate of λ_{EC} is given by [32]. In this approach, the correction to $n_Xh(Q)$ depends on the data block size. In this work, we utilise the approach of [32] to estimate the information leaked during error correction. In particular,

$$\begin{aligned} \lambda_{EC} = & n_Xh(Q) + n_X(1 - Q) \log \left[\frac{(1 - Q)}{Q} \right] \\ & - [F^{-1}(\epsilon_c; n_X, 1 - Q,) - 1] \log \left[\frac{(1 - Q)}{Q} \right] \\ & - \frac{1}{2} \log(n_X) - \log(1/\epsilon_c), \end{aligned} \quad (\text{A1})$$

where n_X is the data block size, Q is the QBER and F^{-1} is the inverse of the cumulative distribution function of the binomial distribution.

Appendix B: Protocol optimisation

We detail the numerical optimisation that we implement for the finite key length. The finite key rate is a complex function of these five protocol parameters: $\{p_X, \mu_1, \mu_2, p_1, p_2\}$, where $p_Z = 1 - p_X$ and $p_3 = 1 - p_1 - p_2$ are fixed by the optimised quantities, and we set $\mu_3 = 0$. We generate an optimised key length by optimising over the parameter space of these five variables. We do so by implementing a constrained numerical optimisation program, which ensures the generated finite key length satisfies the following criteria [30]:

1. $0 < p_X < 1$ (Asymmetric BB84)
2. $0 < p_j < 1$ (Probability axiom for p_j)
3. $0 < \mu_1 < 1$ (Security constraint)
4. $0 < \mu_2 < 1$ (Security constraint)
5. $\mu_2 < \mu_1 - \mu_3$ (Security constraint)
6. $\mu_3 < \mu_2$ (Security constraint)

The security of the key rate derived from the asymmetric, decoy state BB84 protocol has a specific definition. Notably, for small protocol errors, $\epsilon_c, \epsilon_s > 0$, the protocol is $\epsilon_c + \epsilon_s$ -secure if it is ϵ_c -correct and ϵ_s -secret. For the numerical optimisation, we take $\epsilon_c = 10^{-15}$ and $\epsilon_s = 10^{-9}$.

In addition, we take into account some fixed parameters for the numerical optimisation as shown in Table I that define a baseline for system performance. The numerical optimisation is performed separately for different values of Δt , we then chose the value of Δt that yields the largest secret key length, for the particular value of system link efficiency. The full optimisation over $\{P_X, p_1, p_2, \mu_1, \mu_2\}$ and Δt , occurs for each value of system efficiency. For example, in figure 6, each point of the graph corresponds to different optimised parameters.

Appendix C: Asymptotic key length per pass

In this section we give an operational definition for the asymptotic key length per pass and briefly sketch its derivation. One can combine data from multiple satellite passes, and extract a secret key from the combined results. The optimisation over system parameters would then be performed for the combined results, over several passes.

In principle, we can combine results from different satellite orbits. However, for simplicity, here we only consider the case where we combine data from passes with the same orbit and under similar conditions.

Let ℓ_1 be the length of key we extract from a single pass. Naively, one might expect that the length of key for two passes would equal $2\ell_1$. This intuition, however, is false. This is illustrated in Fig. 10, where for a single pass we obtain no key, but a non-zero key is recovered for two or more passes. In this figure, we plotted the key length per pass, which allows us to clearly see the the advantage of combining data. Another thing to note about Fig. 10 is that while there is a gain in combining three or more passes, this gain seems to decrease.

A natural question to ask is: what is largest possible SKL, per pass, that one can obtain by combining arbitrarily many passes? This is given by the quantity $\ell_\infty = \lim_{M \rightarrow \infty} \ell_M/M$, where M is the number of passes and ℓ_M is the SKL one can extract by combining M passes. The key length, ℓ_M , is found using equation (4), together with equations (2)-(5) of [30]. The quantity ℓ_∞ is found by examining the asymptotic scaling of ℓ_M/M . We will not give the complete derivation, but will illustrate the method by looking at the first term: $s_{X,0}/M$.

The estimate for the vacuum counts per pass is [30],

$$\frac{s_{X,0}}{M} = \frac{\tau_0}{\mu_2 - \mu_3} \frac{\mu_2 \Gamma_3 \left(n_{X,3} - \delta_{X,3}^- \right) - \mu_3 \Gamma_2 \left(n_{X,2} + \delta_{X,2}^+ \right)}{M}, \quad (\text{C1})$$

where $n_{X,k}$ is the number of sifted counts in the X-basis, from pulses of intensity k , τ_0 is averaged probability that a vacuum state is transmitted by the laser, $\Gamma_k = \exp(\mu_k)/p_k$ and $\delta_{X,k}^\pm$ are a correction terms resulting from the finite statistics. In [30], $\delta_{X,k}^\pm$ comes from Hoeffding's inequality. In our case, we use the multiplicative Chernoff bound (see equations (9) and (10) of [33]). However, for both the Hoeffding and Chernoff bound,

the asymptotic scaling of $\delta_{X,k}^\pm$ goes $\mathcal{O}(\sqrt{n_X})$. This means that the scaling with the number of satellite passes is $\mathcal{O}(\sqrt{M})$. Hence, $\delta_{X,k}^\pm/M$ scales $\mathcal{O}(1/\sqrt{M})$ and thus tends to zero as $M \rightarrow \infty$. The finite statistics correction terms thus go to zero.

By assumption, each satellite pass is for the same orbit and under similar conditions. We should expect that $n_{X,k}$ equals m times the number of counts for a single pass, $n_{X,k}^{(1)}$. From this observation, we obtain

$$\lim_{M \rightarrow \infty} \frac{s_{X,0}}{M} = \frac{\tau_0}{\mu_2 - \mu_3} \left(\mu_2 \Gamma_3 n_{X,3}^{(1)} - \mu_3 \Gamma_2 n_{X,2}^{(1)} \right) = s_{X,0}^*, \quad (C2)$$

where $s_{X,0}^*$ is the asymptotic estimate of the vacuum counts for a single pass. By following a similar process for each term in ℓ_M/M , we obtain the result

$$\ell_\infty = \left\lfloor s_{X,0}^* + s_{X,1}^* (1 - h(\phi_X^*)) - \lambda_{EC}^\infty \right\rfloor, \quad (C3)$$

where $\phi_X^* = v_{Z,1}^*/s_{Z,1}^*$ is the phase error rate, $s_{X,1}^*$, $s_{Z,1}^*$ and $v_{Z,1}^*$ are respectively, the single pass asymptotic estimates for: the single photon counts in the X basis, the single photon counts in the Z basis and the single photon errors in the Z basis. The expressions for $s_{X,1}^*$, $s_{Z,1}^*$ and $v_{Z,1}^*$ are identical to the equations for the equivalent asymptotic quantities given in Appendix A of [30]. The term λ_{EC}^∞ is the limit of λ_{EC}/M . This depends on how we estimate the information leaked during error correction.

A refined estimate of λ_{EC} is presented in [32]. Equation (5) of [32] gives a upper bound on the asymptotic behaviour of λ_{EC} . Using this expression, we find that $\lambda_{EC}^\infty = n_X^{(1)} h(Q)$, where Q is the QBER for a single pass. When running the numerical code for the asymptotic key length per pass, we set $\lambda_{EC}^\infty = 1.16 n^{(1)} h(Q)$. This was to take account of the fact that even in the asymptotic limit, our error correction protocol might not be perfectly efficient. However, in all other runs, we used the expression for λ_{EC} given in equation (6) of [32].

Rather than looking at the key length per pass, it is also common to consider the key rate, i.e. the number of secret key bits per transmitted pulse. Let N be the total number of pulses transmitted by the satellite during a single pass. The key rate for M passes is just $SKR_M = \ell_M/(MN)$. In the limit of infinitely many passes, the asymptotic key rate is given by $SKR_\infty = \ell_\infty/N$.

We conclude by noting that the asymptotic secret key rate, SKR_∞ , we present is rather different from the one often discussed in the literature. It is more common to calculate an asymptotic key rate for each angle of elevation and then combine the asymptotic key rates in a manner similar to that shown in equation (1). While such an approach is sensible if we extract keys for each angle of elevation, it is not appropriate for the current analysis, where we group all the data for a pass and then extract a key from the combined data.

[1] J. P. Dowling and G. J. Milburn, “Quantum technology: the second quantum revolution,” *Philosophical Transactions of the Royal Society of London. Series A: Mathematical, Physical and Engineering Sciences*, vol. 361, no. 1809, pp. 1655–1674, 2003.

[2] T. J. Proctor, P. A. Knott, and J. A. Dunningham, “Multiparameter estimation in networked quantum sensors,” *Phys. Rev. Lett.*, vol. 120, p. 080501, February 2018.

[3] J. S. Sidhu, Y. Ouyang, E. T. Campbell, and P. Kok, “Tight bounds on the simultaneous estimation of incompatible parameters,” *ArXiv*, December 2019.

[4] J. S. Sidhu and P. Kok, “Geometric perspective on quantum parameter estimation,” *AVS Quantum Science*, vol. 2, p. 014701, February 2020.

[5] V. Scarani, H. Bechmann-Pasquinucci, N. J. Cerf, M. Dušek, N. Lütkenhaus, and M. Peev, “The security of practical quantum key distribution,” *Rev. Mod. Phys.*, vol. 81, pp. 1301–1350, September 2009.

[6] S. Pirandola, U. L. Andersen, L. Banchi, M. Berta, D. Bunandar, R. Colbeck, D. Englund, T. Gehring, C. Lupo, C. Ottaviani, *et al.*, “Advances in quantum cryptography.” unpublished, June 2019.

[7] E. Knill, R. Laflamme, and G. J. Milburn, “A scheme for efficient quantum computation with linear optics,” *Nature*, vol. 409, pp. 46–52, January 2001.

[8] J. F. Fitzsimons, “Private quantum computation: an introduction to blind quantum computing and related protocols,” *NPJ Quantum Inf.*, vol. 3, p. 23, May 2017.

[9] S. Wehner, D. Elkouss, and R. Hanson, “Quantum internet: A vision for the road ahead,” *Science*, vol. 362, October 2018.

[10] P. C. Humphreys, M. Barbieri, A. Datta, and I. A. Walmsley, “Quantum enhanced multiple phase estimation,” *Phys. Rev. Lett.*, vol. 111, p. 070403, August 2013.

[11] P. Kómár, E. M. Kessler, M. Bishof, L. Jiang, A. S. Sørensen, J. Ye, and M. D. Lukin, “A quantum network of clocks,” *Nat. Phys.*, vol. 10, pp. 582–587, June 2014.

[12] E. Polino, M. Riva, M. Valeri, R. Silvestri, G. Corrielli, A. Crespi, N. Spagnolo, R. Osellame, and F. Sciarrino, “Experimental multiphase estimation on a chip,” *Optica*, vol. 6, pp. 288–295, March 2019.

[13] X. Guo, C. R. Breum, J. Borregaard, S. Izumi, M. V. Larsen, T. Gehring, M. Christandl, J. S. Neergaard-Nielsen, and U. L. Andersen, “Distributed quantum sensing in a continuous-variable entangled network,” *Nat. Phys.*, vol. 16, pp. 281–284, December 2020.

[14] E. O. Ilo-Okeke, L. Tessler, J. P. Dowling, and T. Byrnes, “Remote quantum clock synchronization without synchronized clocks,” *NPJ Quantum Inf.*, vol. 4, p. 40, June 2018.

[15] R. Jozsa, D. S. Abrams, J. P. Dowling, and C. P. Williams, “Quantum clock synchronization based on shared prior entanglement,” *Phys. Rev. Lett.*, vol. 85, pp. 2010–2013, August 2000.

[16] T. Qian, J. Bringewatt, I. Boettcher, P. Bienias, and A. V. Gorshkov, “Optimal measurement of field properties with quantum sensor networks.” unpublished, November 2020.

[17] H.-L. Yin, T.-Y. Chen, Z.-W. Yu, H. Liu, L.-X. You, Y.-H. Zhou, S.-J. Chen, Y. Mao, M.-Q. Huang, W.-J. Zhang, H. Chen, M. J. Li, D. Nolan, F. Zhou, X. Jiang, Z. Wang, Q. Zhang, X.-B. Wang, and J.-W. Pan, “Measurement-device-independent quantum key distribution over a 404 km optical fiber,” *Phys. Rev. Lett.*, vol. 117, p. 190501, Nov 2016.

[18] A. Boaron, G. Boso, D. Rusca, C. Vulliez, C. Autebert, M. Caloz, M. Perrenoud, G. Gras, F. Bussières, M.-J. Li, D. Nolan, A. Martin, and H. Zbinden, “Secure quantum key dis-

tribution over 421 km of optical fiber,” *Phys. Rev. Lett.*, vol. 121, p. 190502, Nov 2018.

[19] A. Boaron, D. Rusca, G. Boso, R. Houlmann, F. Grünenfelder, C. Vulliez, M. Caloz, M. Perrenoud, G. Gras, C. Autebert, *et al.*, “Progress on quantum key distribution using ultralow loss fiber,” in *Optical Fiber Communication Conference*, pp. M4A-5, Optical Society of America, 2020.

[20] J.-P. Chen, C. Zhang, Y. Liu, C. Jiang, W. Zhang, X.-L. Hu, J.-Y. Guan, Z.-W. Yu, H. Xu, J. Lin, M.-J. Li, H. Chen, H. Li, L. You, Z. Wang, X.-B. Wang, Q. Zhang, and J.-W. Pan, “Sending-or-not-sending with independent lasers: Secure twin-field quantum key distribution over 509 km,” *Phys. Rev. Lett.*, vol. 124, p. 070501, Feb 2020.

[21] Y. Wu, J. Liu, and C. Simon, “Near-term performance of quantum repeaters with imperfect ensemble-based quantum memories,” *Physical Review A*, vol. 101, no. 4, p. 042301, 2020.

[22] R. Hughes, W. Buttler, P. Kwiat, S. Lamoreaux, G. Luther, G. Morgan, J. Nordholt, and C. Peterson, “Quantum cryptography for secure free-space communications,” *Proc SPIE*, vol. 3615, pp. 98–103, October 1999.

[23] C. Kurtsiefer, P. Zarda, M. Halder, H. Weinfurter, P. M. Gorman, P. R. Tapster, and J. G. Rarity, “A step towards global key distribution,” *Nature*, vol. 419, no. 6906, pp. 450–450, 2002.

[24] D. K. Oi, A. Ling, G. Vallone, P. Villoresi, S. Greenland, E. Kerr, M. Macdonald, H. Weinfurter, H. Kuiper, E. Charbon, and R. Ursin, “Cubesat quantum communications mission,” *EPJ Quantum Technology*, vol. 4, no. 1, p. 6, 2017.

[25] L. Mazzarella, C. Lowe, D. Lowndes, S. Joshi, S. Greenland, D. McNeil, C. Mercury, M. Macdonald, J. Rarity, and D. Oi, “Quarc: Quantum research cubesat—a constellation for quantum communication,” *Cryptography*, vol. 4, February 2020.

[26] M. Polnik, L. Mazzarella, M. Di Carlo, D. K. Oi, A. Riccardi, and A. Arulselvan, “Scheduling of space to ground quantum key distribution,” *EPJ Quantum Technology*, vol. 7, no. 1, p. 3, 2020.

[27] M. Gündoğan, J. S. Sidhu, V. Henderson, L. Mazzarella, J. Wolters, D. K. Oi, and M. Krutzik, “Space-borne quantum memories for global quantum communication.” unpublished, June 2020.

[28] P. Jianwei, “Progress of the quantum experiment science satellite (quess) micius project,” *Chin. J. Space Science*, vol. 38, no. 5, pp. 604–609, 2018.

[29] M. Tomamichel, C. C. W. Lim, N. Gisin, and R. Renner, “Tight finite-key analysis for quantum cryptography,” *Nat. Commun.*, vol. 3, p. 634, January 2012.

[30] C. C. W. Lim, M. Curty, N. Walenta, F. Xu, and H. Zbinden, “Concise security bounds for practical decoy-state quantum key distribution,” *Phys. Rev. A*, vol. 89, p. 022307, February 2014.

[31] D. Rusca, A. Boaron, F. Grünenfelder, A. Martin, and H. Zbinden, “Finite-key analysis for the 1-decoy state qkd protocol,” *Appl. Phys. Lett.*, vol. 112, p. 171104, April 2018.

[32] M. Tomamichel, J. Martínez-Mateo, C. Pacher, and D. Elkouss, “Fundamental finite key limits for one-way information reconciliation in quantum key distribution,” *Quant. Inf. Proc.*, vol. 16, p. 280, October 2017.

[33] H.-L. Yin, M.-G. Zhou, J. Gu, Y.-M. Xie, Y.-S. Lu, and Z.-B. Chen, “Tight security bounds for decoy-state quantum key distribution,” *Sci. Rep.*, vol. 10, p. 14312, August 2020.

[34] J.-P. Bourgoin, E. Meyer-Scott, B. L. Higgins, B. Helou, C. Erven, H. Huebel, B. Kumar, D. Hudson, I. DSouza, R. Girard, R. Laflamme, and T. D. Jennewein, “A comprehensive design and performance analysis of low earth orbit satellite quantum communication,” *New Journal of Physics*, vol. 15, no. 2, p. 023006, 2013.

[35] J.-P. Bourgoin, N. Gigov, B. L. Higgins, Z. Yan, E. Meyer-Scott, A. K. Khandani, N. Lütkenhaus, and T. Jennewein, “Experimental quantum key distribution with simulated ground-to-satellite photon losses and processing limitations,” *Physical Review A*, vol. 92, no. 5, p. 052339, 2015.

[36] M. Curty, F. Xu, W. Cui, C. C. W. Lim, K. Tamaki, and H.-K. Lo, “Finite-key analysis for measurement-device-independent quantum key distribution,” *Nat. Commun.*, vol. 5, p. 3732, 2014.

[37] D. Bacco, M. Canale, N. Laurenti, G. Vallone, and P. Villoresi, “Experimental quantum key distribution with finite-key security analysis for noisy channels,” *Nature communications*, vol. 4, no. 1, pp. 1–8, 2013.

[38] H. Y. Lim, T. Vergoossen, R. Bedington, X. Bai, A. Villar, A. Lohrmann, N. H. Nhung, S. Barraclough, J. Vennik, D. Griffin, and A. Ling, “Thermo-mechanical design for a miniaturized quantum light source on board the spooqy-1 cubesat.” unpublished, June 2020.

[39] D. Vasylyev, W. Vogel, and F. Moll, “Satellite-mediated quantum atmospheric links,” *Physical Review A*, vol. 99, no. 5, p. 053830, 2019.

[40] J. Yin, Y. Cao, Y.-H. Li, S.-K. Liao, L. Zhang, J.-G. Ren, W.-Q. Cai, W.-Y. Liu, B. Li, H. Dai, *et al.*, “Satellite-based entanglement distribution over 1200 kilometers,” *Science*, vol. 356, no. 6343, pp. 1140–1144, 2017.

[41] V. C. Usenko, B. Heim, C. Peuntinger, C. Wittmann, C. Marquardt, G. Leuchs, and R. Filip, “Entanglement of gaussian states and the applicability to quantum key distribution over fading channels,” *New J. Phys.*, vol. 14, no. 9, p. 093048, 2012.

[42] N. Hosseiniidehaj, N. Walk, and T. C. Ralph, “Composable finite-size effects in free-space cv-qkd systems,” *arXiv preprint arXiv:2002.03476*, 2020.

[43] J. Yin, Y.-H. Li, S.-K. Liao, M. Yang, Y. Cao, L. Zhang, J.-G. Ren, W.-Q. Cai, W.-Y. Liu, S.-L. Li, *et al.*, “Entanglement-based secure quantum cryptography over 1,120 kilometres,” *Nature*, vol. 582, no. 7813, pp. 501–505, 2020.

[44] C. Liorni, H. Kampermann, and D. Bruß, “Satellite-based links for quantum key distribution: beam effects and weather dependence,” *New Journal of Physics*, vol. 21, no. 9, p. 093055, 2019.

[45] D. Vasylyev, A. Semenov, and W. Vogel, “Atmospheric quantum channels with weak and strong turbulence,” *Physical review letters*, vol. 117, no. 9, p. 090501, 2016.

[46] L. C. Andrews and R. L. Phillips, *Laser beam propagation through random media*. SPIE Press, 2005.

[47] A. Berk, P. Conforti, R. Kennett, T. Perkins, F. Hawes, and J. van den Bosch, “Modtran6: a major upgrade of the modtran radiative transfer code,” in *Proc. SPIE*, vol. 9088, 6 2014.

[48] S. Pirandola, “Satellite quantum communications: Fundamental bounds and practical security.” unpublished, December 2020.

[49] T. Vergoossen, S. Loarte, R. Bedington, H. Kuiper, and A. Ling, “Modelling of satellite constellations for trusted node qkd networks,” *Acta Astronautica*, 2020.

[50] H.-K. Lo, H. F. Chau, and M. Ardehali, “Efficient quantum key distribution scheme and a proof of its unconditional security,” *Journal of Cryptology*, vol. 18, no. 2, pp. 133–165, 2005.

[51] I. Aharonovich, D. Englund, and M. Toth, “Solid-state single-photon emitters,” *Nature Photonics*, vol. 10, no. 10, pp. 631–641, 2016.

[52] D. Gottesman, H.-K. Lo, N. Lütkenhaus, and J. Preskill, “Security of quantum key distribution with imperfect devices,” in *International Symposium on Information Theory, 2004. ISIT 2004. Proceedings.*, p. 136, IEEE, 2004.

[53] R. Renner, *Security of Quantum Key Distribution*. PhD thesis, Swiss Federal Institute of Technology, Zurich, January 2006. unpublished.

- [54] I. Holzman and Y. Ivry, "Superconducting nanowires for single-photon detection: Progress, challenges, and opportunities," *Advanced Quantum Technologies*, vol. 2, no. 3-4, p. 1800058, 2019.
- [55] F. Ceccarelli, G. Acconcia, A. Gulinatti, M. Ghioni, I. Rech, and R. Osellame, "Recent advances and future perspectives of single-photon avalanche diodes for quantum photonics applications," *arXiv preprint arXiv:2010.05613*, 2020.
- [56] C. H. Bennett and G. Brassard, "Quantum cryptography: Public key distribution and coin tossing," *Proc. IEEE Int. Conf. Comput., Syst. Signal Process.*, pp. 175–179, 1984.
- [57] G. Brassard, N. Lütkenhaus, T. Mor, and B. C. Sanders, "Limitations on practical quantum cryptography," *Phys. Rev. Lett.*, vol. 85, pp. 1330–1333, August 2000.
- [58] W.-Y. Hwang, "Quantum key distribution with high loss: Toward global secure communication," *Phys. Rev. Lett.*, vol. 91, p. 057901, August 2003.
- [59] X.-B. Wang, "Beating the photon-number-splitting attack in practical quantum cryptography," *Phys. Rev. Lett.*, vol. 94, p. 230503, June 2005.
- [60] H.-K. Lo, X. Ma, and K. Chen, "Decoy state quantum key distribution," *Phys. Rev. Lett.*, vol. 94, p. 230504, June 2005.
- [61] X. Ma, B. Qi, Y. Zhao, and H.-K. Lo, "Practical decoy state for quantum key distribution," *Phys. Rev. A*, vol. 72, p. 012326, July 2005.
- [62] J. Hasegawa, M. Hayashi, T. Hiroshima, and A. Tomita, "Security analysis of decoy state quantum key distribution incorporating finite statistics," unpublished, July 2007.
- [63] R. Y. Q. Cai and V. Scarani, "Finite-key analysis for practical implementations of quantum key distribution," *New J. Phys.*, vol. 11, p. 045024, April 2009.
- [64] M. Hayashi and R. Nakayama, "Security analysis of the decoy method with the bennett–brassard 1984 protocol for finite key lengths," *New J. Phys.*, vol. 16, p. 063009, June 2014.
- [65] Z. Zhang, Q. Zhao, M. Razavi, and X. Ma, "Improved key-rate bounds for practical decoy-state quantum-key-distribution systems," *Phys. Rev. A*, vol. 95, p. 012333, January 2017.